ARCHIVES OF ELECTRICAL ENGINEERING VOL. 68(1), pp. 115–133 (2019)

DOI 10.24425/aee.2019.125984

# Cogging torque and torque ripple analysis of permanent magnet flux-switching machine having two stators

CHUKWUEMEKA CHIJIOKE AWAH[1], OGBONNAYA INYA OKORO[1], EDWARD CHIKUNI[2]

[1] *Department of Electrical and Electronics Engineering*
*Michael Okpara University of Agriculture*
*PMB 7267 Umudike, Nigeria*

[2] *Department of Electrical Engineering, University of Zimbabwe, Harare, Zimbabwe*
*e-mails: awahchukwuemeka@gmail.com, {profogbonnayaokoro/echikuni}@ieee.org*

(Received: 13.06.2018, revised: 31.10.2018)

**Abstract:** The analysis of cogging torque, torque ripple and total harmonic distortion of a permanent magnet (PM) flux-switching machine having separate excitation stators is presented in this study. Further, the effect of unbalanced magnetic force (UMF) on the rotor of this machine is also investigated. A comparison of the analysed machine having different rotor pole configurations is also given. The analysis shows that the largest cogging torque, torque ripple as well as total harmonic distortion (THD) are obtained in the four-rotor-pole machine while the least of THD and torque ripple effects is seen in the thirteen-rotor-pole machine. Furthermore, the evaluation of the radial magnetic force of the machines having an odd number of rotor poles shows that the investigated machine having a five-rotor-pole number exhibits the highest value of UMF, while the smallest amount of UMF is obtained in an eleven-rotor-pole machine. Similarly, it is observed that the machines having an even number of rotor poles exhibit a negligible amount of UMF compared to the ones of the odd number of rotor poles.

**Key words:** cogging torque, torque ripple, separate stators, and unbalanced magnetic force

## 1. Introduction

Undesirable qualities such as cogging torque, torque ripple and unbalanced magnetic force (UMF) are parasitic effects which reduce not just the output torque but the life span of a given electric machine; in addition, it causes noise and vibration in the system. Therefore, a precise study of these effects should be investigated. Various methods such as rotor skewing, the optimization of a magnet pole arc, and the introduction of a multi-tooth on the stator of interior permanent magnet (IPM) machines have been proven to be effective in reducing the cogging torque as detailed in [1]. It is noted in particular that the additional slots created by the multi-toothed structure will result in

more phase-shifted harmonic waveforms, whose resultant effect will cancel out most of the torque harmonic contents on summation. The influence of permanent magnet (PM) segmentation, as well as the effect of angular displacement between the segmented PMs on the amplitude of cogging torque of a given surface-mounted PM machine is investigated in [2]. The studies show that, the smaller the shift angle between the sets of partitioned PMs, the higher the magnitude of its cogging torque. However, a high reduction of cogging torque is achieved as the segmented portions of the magnet are varied over the range of integers, and an optimum number of 4-segments per magnet pole is realized.

Similarly, [3] showed that by selecting an appropriate stator and rotor pole configuration and by adopting an optimal rotor pole width as well as implementation of rotor skewing, a significant amount of both the cogging torque and torque ripple of a switched flux PM machine could be minimized; however with some trade-off of the output torque. The angular displacement of slot-openings in a PM machine is a major determinant in calculating the amplitude of its cogging torque as presented in [4]. The effective reduction of cogging torque could be realized by dividing the stator slots into different phase-groups having opposite angular polarity. Nevertheless, this may lead to a little reduction in the fundamental value of electromotive force (EMF) and thus, on the overall machine performance.

More so, it is shown in [5] that the torque ripple of interior permanent magnet (IPM) machines could be reduced greatly by increasing the number of its phases i.e. the use of multi-phase systems, in addition to the appropriate selection of stator and rotor pole combinations. Moreover, it is proven in [6] that by adopting an optimal teeth topology in a transverse flux PM machine, then, both the unbalanced magnetic force and torque ripple could be substantially reduced. Similarly, an improved doubly-salient PM (DSPM) machine having an outer-rotor configuration and capable of suppressing the self-inductance which in turn produces lower torque ripple compared to the conventional DSPM machines is proposed and analysed in [7].

Further, the eccentricity effect which is the root cause of unbalanced magnetic force (UMF) in an electric machine is demonstrated in [8]. It is noted that, the impact of this feature is significantly large for a magnetless machine, in a low-load situation compared to the predictions at high current, due to the non-linearity that exists under such heavy load conditions. In contrast, these non-linear effects have pronounced influence on the amount of UMF of synchronous alternators as noted in [9].

Furthermore, the UMF of magnetically-geared machines could be completely eliminated as illustrated in [10], by choosing the correct number of slots and PM pole-pairs. Moreover, an examination of the effects of winding topologies shown in [11] reveals that fractional slot PM machines having single-layer windings are characterized by a high amount of UMF and vibration on both on-load and open-circuit conditions, even in the absence of rotor eccentricity.

In the light of the foregoing, therefore, the effect of cogging torque, torque ripple, total harmonic distortion as well as unbalanced magnetic force of a double-stator PM machine under different load conditions is presented in this paper. Special consideration is also given to its different number of rotor poles. Fig. 1 shows the schematic of the traditional E-core flux-switching PM machine, the geometrical dimensions and the 3D-FEA structural diagram of the developed machine with its mesh lines. Note that the windings of the developed machine are coated with varnish in order to hold it firmly on the insulated stator.

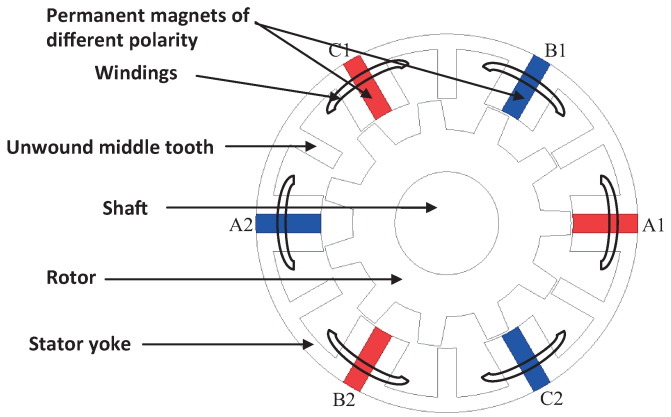


(a) Conventional E-core SFPM machine having 11-rotor pole and 6-stator pole (E-core SFPM 6/11)

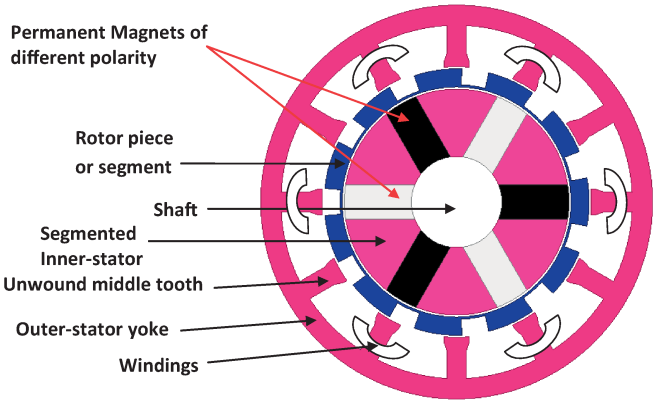


(b) 2D geometric view

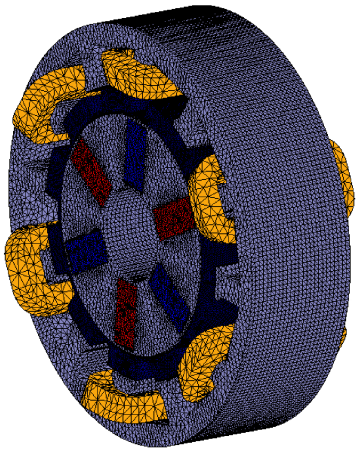

(c) 3D FEA mesh distribution

Fig. 1. Structural view of the developed machine with mesh contour

## 2. Methodology and working principle

The investigated 90 mm stator diameter sized machine has 72 turns per phase. The whole results in this paper are predicted with the aid of 2D-finite element software (MAXWELL-ANSOFT/ANSYS).

The developed machine is basically a flux-switching permanent magnet machine with two independent stators. It is similar to the conventional E-core SFPM machine of Fig. 1(a), however, with the permanent magnets relocated to the partitioned inner-stator segments. The outer-stator is equipped with three phase windings and injected with sinusoidal alternating currents (ACs). The applied phase current waveform is such that it is in phase with the induced phase EMF waveform. Meanwhile, the segmented inner-stator houses the permanent magnets (PMs). The flux-focusing effect from the spoke-mounted PMs which enhances both the airgap flux-density as well as the output electromagnetic torque is adopted in this machine design. The PMs are located such that each adjacent PM has a reverse polarity to the PM next to it. Moreover, the magnetic fields produced by both the stator windings and the permanent magnets are independent of each other, hence, their magnetic paths do not interfere with each other. The above assertion on a magnetic path feature is common amongst the flux-switching PM machines as stated in [12] and [13]. This feature reduces the risk of PM demagnetization which would have resulted from the armature reaction of the stator windings. Just like in the conventional flux-switching PM machines, the produced flux reverses its direction of flow twice in a single electric cycle, thus giving rise to the bipolar flux-linkage and induced electromotive force waveforms obtainable in the developed machine. More so, the EMF and flux-linkage waveforms of the developed machine are essentially sinusoidal, which is a good control property. This is also a typical characteristic of the flux-switching PM machine as pointed out in [14] and [15]. In addition, the magnetic field distributions of the analysed machines under different conditions, as well as the corresponding flux-linkage and back-EMF waveforms are presented for clarity.

The investigated machine is excited by the PMs even under open-circuit condition. In a half electric period, the cup-rotor rotates and depending on the different alignment positions of the rotor pole with the slot-opening and stator pole, coil flux-linkage having minimum, zero and maximum values which corresponds to the negative $d$-axis, $q$-axis and positive $d$-axis positions of the rotor, respectively, are thus produced. A bipolar coil flux-linkage is obtained over a complete cycle of 360° (electrical degrees). The resultant phase flux-linkage under no-load is displayed in Fig. 4. Eventually, a periodic change of the flux-linkage will result to induced bipolar electromotive force (EMF) on the armature windings. Consequent upon that, electromagnetic torque and power would be developed owing to the injected AC phase currents which, as earlier mentioned, would be in phase with the EMF, at the same operating frequency.

The inner stator space of the developed machine is well utilized, since the PMs are relocated in the inner stator space unlike the conventional flux-switching PM machine in which the PMs and the windings are both situated on the same stator. It is worth noting that, the investigated machine is a dual-airgap machine. Although double-airgap PM machines have manufacturing complexity with relatively higher production cost; however, it has the advantage of producing larger torque density comparable to their corresponding single-airgap equivalents as stated in [16, 17] and [18]. The above mentioned merit of enhanced torque density is the driving force behind this design. Further, a double-stator PM machine produces larger torque compared to

their single-stator counterparts; this characteristic is noted and justified in [19, 20] and [21], respectively. Moreover, the investigated machine has a good fault-tolerant feature owing to the physical isolation of the phase windings from each other which would reduce the occurrence of short-circuit faults, albeit with large undesirable unbalanced magnetic force acting on its rotor. Generally speaking, the developed machine would be more suited in high torque low speed direct-drive applications; in particular, for in-wheel purposes in the aerospace and automobile industries. Nevertheless, the flux-switching PM machines are known to possess a high amount of cogging torque when compared with other PM machines.

The first assumption in this design is based upon the fact that the copper loss is usually a dominant loss component in a given electric machine compared to the core losses i.e. copper loss $\gg$ iron loss. Moreover, initial results of the unoptimized machine model gave an output of about 2 Nm. Note that, the machine is operated at a low speed of 400 rpm. The interest is to develop a model with over 70% efficiency; hence, with negligible iron loss value, the efficiency is given in (1).

$$\eta = \frac{\omega T}{\omega T + \text{copper loss}} 100\%. \tag{1}$$

Consequently,

$$\omega T = 400 \text{ rpm} \left(\frac{2\pi}{60}\right) 2 \text{ N.m} = 84 \text{ W}, \tag{2}$$

where $\omega$ = angular speed (r.p.s), and $T$ = torque (N.m).

Thus, the initial estimated efficiency, $\eta$ is approximately 74%, which is within the design target. Overall, the efficiency of the optimized model is predicted with a more accurate expression given in (3).

$$\eta = \frac{\omega T}{\omega T + \text{copper loss} + \text{core loss} + \text{eddy current loss}} 100\%. \tag{3}$$

Further, the optimization of the machine geometries including the split-ratio, which is given by the ratio of the outer airgap radius to the outer radius of the machine, is carried out by employing the inherent genetic algorithm incorporated in the ANSYS/ANSOFT-MAXWELL finite element software at a fixed copper loss value of (30 W) with also a goal to achieve the largest average torque. One essential condition satisfied during the optimization process is given in [22] and expressed in (4), such that the available slot area is directly proportional to the square of the number of turns, for a given current.

$$N \propto \sqrt{S_A}, \tag{4}$$

where $N$ is the number of turns and $S_A$ is the available slot area.

Note that in flux-switching PM machines, it is feasible to work with a different number of rotor poles and not pole pairs obtainable in other PM machines. Essentially, the effect of the number of rotor poles on the investigated machine parameters is considered in this work. Also, the application of each of the machine topology is the same.

The operating frequency of a flux-switching PM machine is given in (5), as stated in [23].

$$f = \frac{N_r n_r}{60}, \tag{5}$$

where $N_r$ is the rotor pole number, and $n_r$ is the rotating speed (rpm).

It is worth noting that, the order of cogging torque, $N_{cog}$ of the developed machine is given in Equation (6), as noted in [24].

$$N_{cog} = \frac{LCM(P, N_r)}{N_r}, \tag{6}$$

where $P$ is the stator-mounted PM pole pair, $N_r$ is the rotor pole number, $LCM$ is the lowest common multiple.

Moreover, the magnitude of the torque ripple in the investigated machine is predicted with the expression in Equation (7).

$$T_{\text{ripple}} = \frac{T_{\max} - T_{\min}}{T_{\text{avg}}} 100\%, \tag{7}$$

where $T_{\max}$, $T_{\min}$, and $T_{\text{avg}}$ the maximum, minimum and average torque respectively.

Similarly, the total harmonic distortion (THD) of the voltage in the analysed machine is evaluated using Equation (8).

$$\text{THD} = \frac{\sqrt{E_2^2 + E_3^2 + \ldots + E_n^2}}{E_1}, \tag{8}$$

where: $E_1$ is the fundamental magnitude of the induced electromotive force, $E_2$, $E_3$, ..., $E_n$ are the sub-harmonic voltages, $n = 59$ in this study, since the time-stepping rotation of the machine is calculated over 60-point intervals in a single electric cycle.

The parameters of the analysed machine are listed in Table 1.

Table 1. Parameters of the investigated machine

| **Element** | **Value** |
|---|---|
| Number of phases, m | 3 |
| Operating speed (rpm) | 400 |
| Outer stator diameter (mm) | 90 |
| Air-gap length (mm) | 0.5 |
| Stack length (mm) | 25 |
| PM residual flux density | 1.2T |
| Permanent magnet grade | N38SH (NdFeB) |
| Laminated rotor and stator sheet | Silicon Steel_1008 |
| Relative permeability | 1.05 |
| No. of turns/coil | 36 |
| Coils/phase | 2 |
| Total number of turns per phase | 72 |

The magnetic field distributions of the analysed machine with its corresponding flux-linkage waveforms under different conditions of frozen permeability analysis are depicted in Figs. 2 and 3,

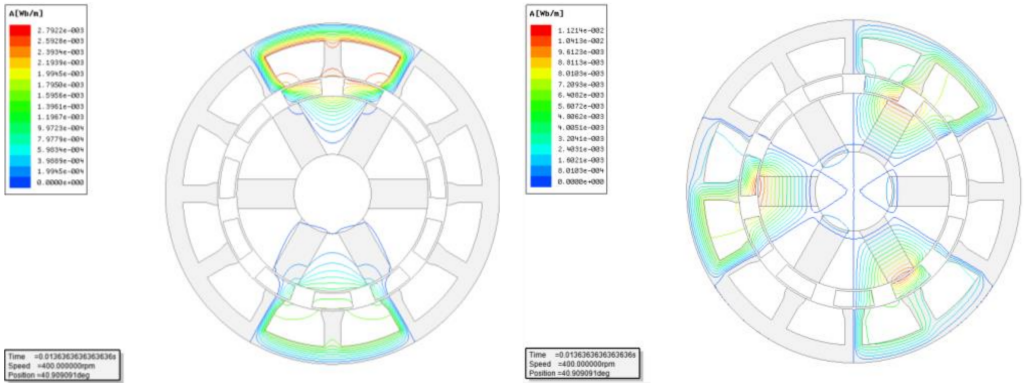

(a) Fields with only external windings excited, 15 A (b) Fields with only PMs excited on open-circuit

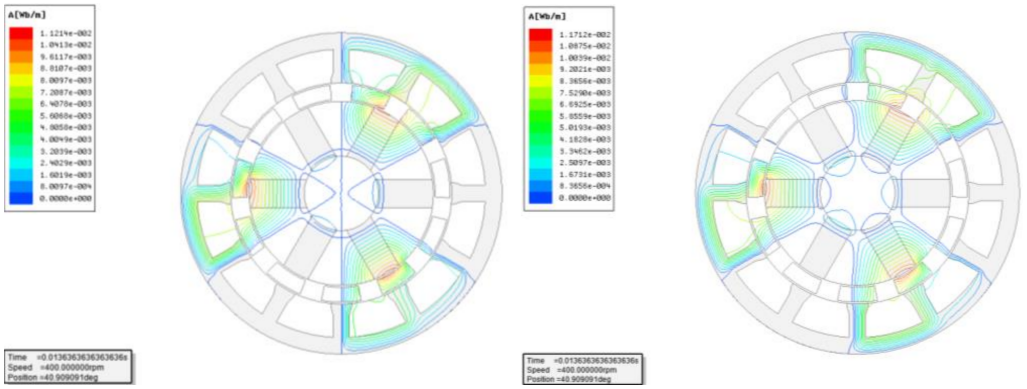

(c) Resultant fields by both sources on open-circuit (d) Resultant fields by both sources at 15 A

Fig. 2. Magnetic field distributions, 11-rotor pole

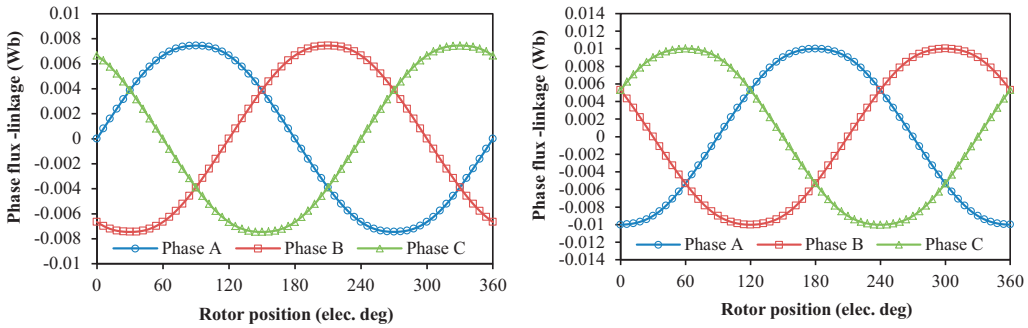


(a) Fields with only external windings excited, 15 A (b) Fields with only PMs excited on open-circuit

Fig. 3.

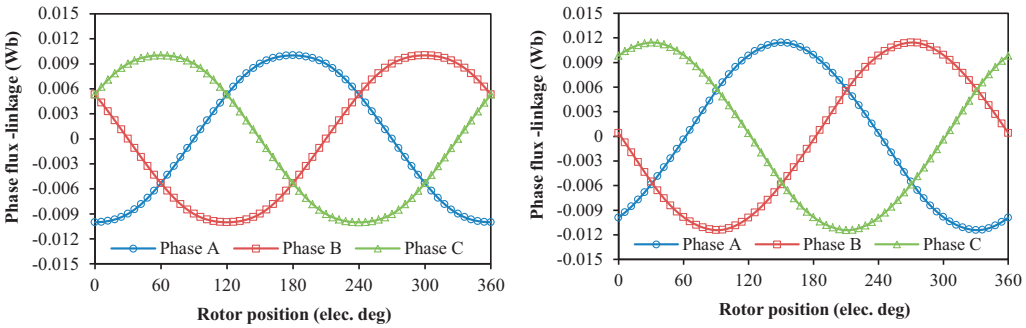


(c) Resultant fields by both sources on open-circuit (d) Resultant fields by both sources at 15 A

Fig. 3. Comparison of phase flux-linkage under different conditions, 11-rotor pole

respectively. It is worth noting that the permanent magnets made greater flux contribution than the excited windings.

Similarly, the open circuit Phase A flux-linkage and back-EMF waveforms of the developed machine operated at 400 rpm is shown in Fig. 4, which confirms that the waveforms are both sinusoidal and symmetrical about the rotor position.

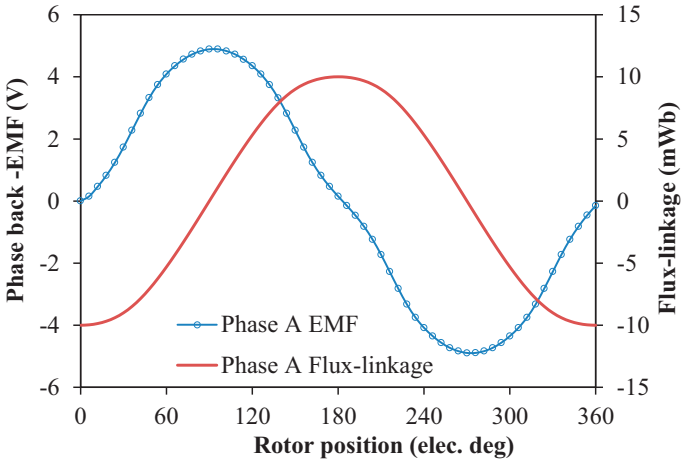


Fig. 4. Comparison of phase A flux-linkage and EMF by both sources, open circuit

## 3. Torque and total harmonic distortion

The relationship between the stator teeth number, $N_{st}$ and the number of magnet poles, $N_{pm}$ is given in Equation (9); however, the windings are wound on half of the total stator teeth number i.e. on every alternate tooth.

$$N_{st} = 2N_{pm}\,. \tag{9}$$

The cogging torque waveforms and spectra of the analysed machines are depicted in Fig. 5. It is observed that, the even-rotor pole machines, especially the 4-pole machine, seem to possess a significant amount of cogging torque.

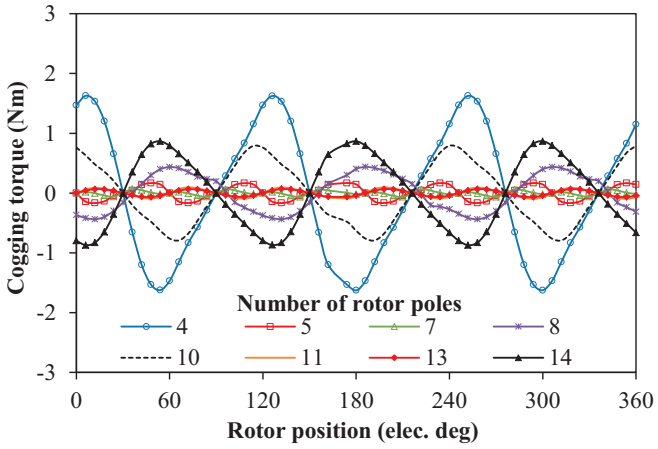


(a) Waveforms

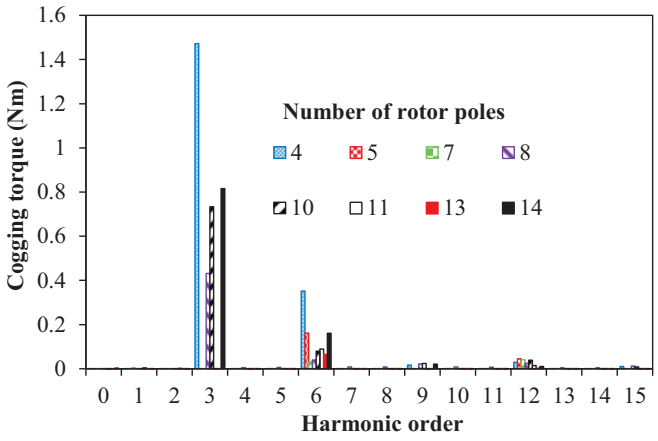


(b) Spectra

Fig. 5. Comparison of cogging torque in analysed machines

Furthermore, the effect of magnet width, the slot opening/tooth pitch ratio, as well as the stator tooth width on the cogging torque of the developed machine is given in Figs. 6–8. Though due to space limitation, we have limited the plots to that of only one rotor pole configuration i.e. the 11-rotor pole structure. Moreover, the optimum values of these design parameters which would yield the minimum amplitude of cogging are listed in Table 2. However, it should be noted that these optimum values capable of yielding the least values of cogging torque may affect the output average torque of the compared machines, if adopted. Hence, there is a need for a compromise

to be reached, depending on the design objective and target. More importantly, the nature of the rotor and the airgap asymmetry as well as the shapes of the design parameters could influence the magnitude of cogging of a given flux-switching PM machine, as investigated and validated in [25] and [26], respectively.

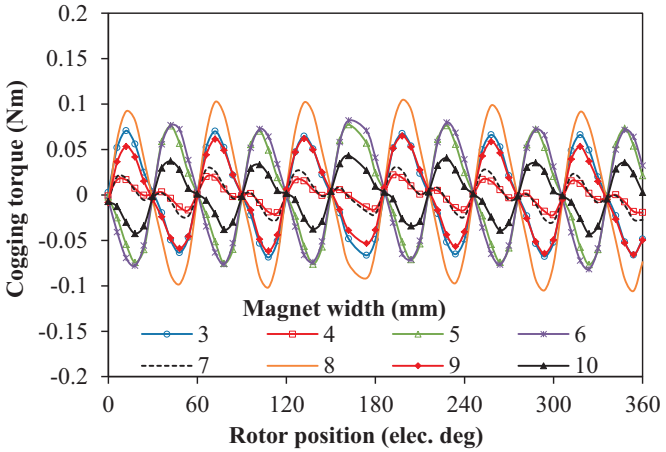


Fig. 6. Comparison of the effect of magnet width on cogging torque, 11-rotor pole

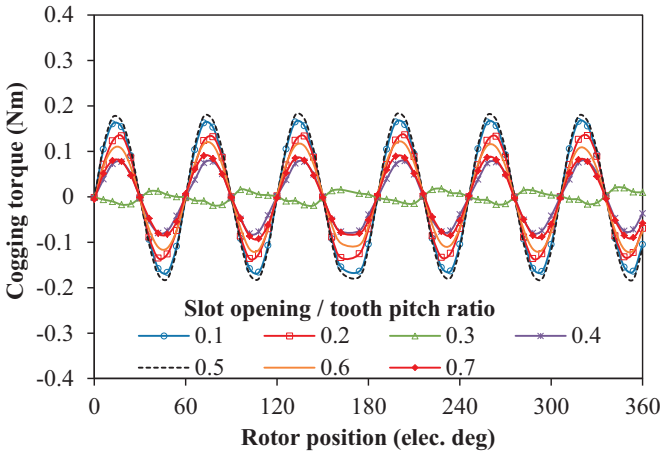


Fig. 7. Comparison of the effect of slot opening/tooth pitch ratio on cogging torque, 11-rotor pole

Torque ripple and total harmonic distortion (THD) curves at different copper loss conditions are shown in Figs. 9 and 10, respectively. The results in Fig. 9 show that, the even-rotor pole machines exhibit the largest amount of torque ripple at all conditions. The 4-pole machine has

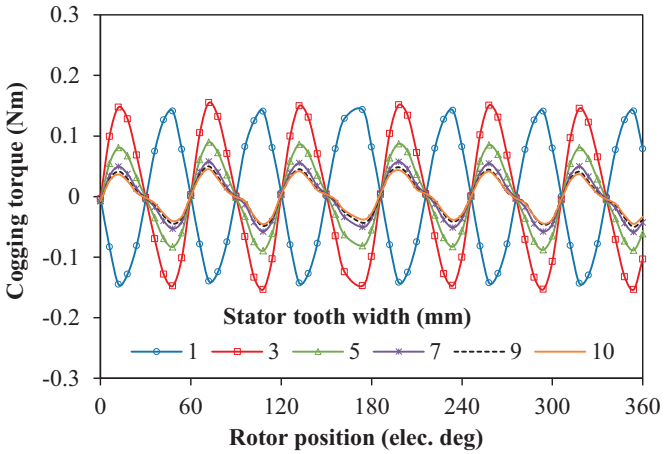


Fig. 8. Comparison of the effect of stator tooth width on cogging torque, 11-rotor pole

the highest value of torque ripple and THD compared to its counterparts. The machines with low THD indicate that they have more sinusoidal back-EMF waveforms and thus fewer harmonics.

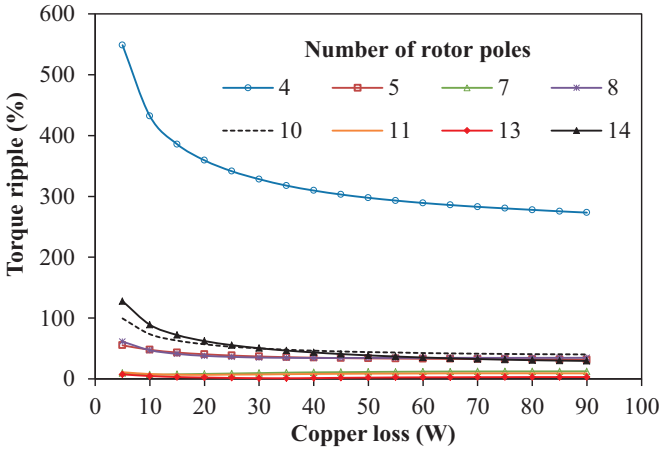


Fig. 9. Variation of torque ripple with copper loss

The vertical axis of Fig. 10 shows the total harmonic distortion component of the voltage. However, the average torque of the machine will differ at each copper loss value. For example, at a value of 30 W, the finite element analysis (FEA) predicted average torque for each of the rotor pole numbers is listed in Table 2. The ratio of the peak-to-peak value of cogging torque to the average torque of the compared machines is also itemized in Table 2. The result shows that the machine having a 4-rotor pole configuration has a very poor result, possibly due to its high

harmonic content. Although, it is noted in [26] that flux-switching PM machine exhibit a larger amount of cogging torque compared to other PM machines.

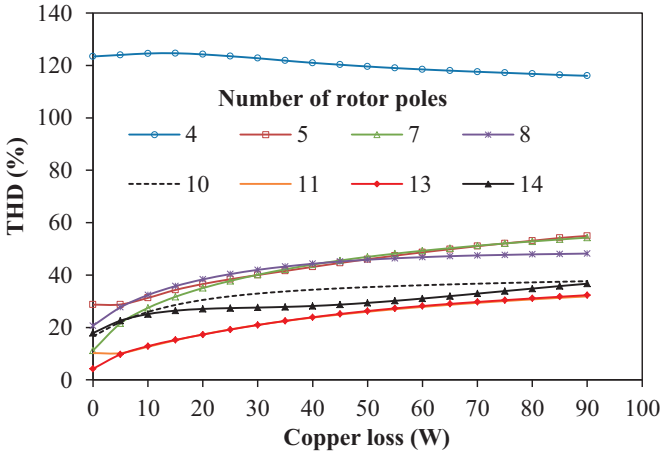


Fig. 10. Comparison of total harmonic distortion against copper loss

Table 2. Torque values of investigated machine

| Number of rotor poles | 4 | 5 | 7 | 8 | 10 | 11 | 13 | 14 |
|---|---|---|---|---|---|---|---|---|
| Average torque (Nm) | 1.44 | 2.28 | 3.01 | 3.17 | 3.82 | 4.15 | 4.07 | 3.07 |
| Torque density (kNm/m$^3$) | 8.84 | 14.33 | 18.94 | 19.97 | 23.89 | 26.12 | 25.56 | 19.38 |
| Magnet eddy current loss (W) | 2.93 | 1.14 | 1.05 | 1.41 | 2.18 | 2.1 | 2.76 | 7.07 |
| Magnet width (mm) | 4 | | | | | | | |
| Slot opening/tooth pitch ratio | 0.3 | | | | | | | |
| Stator tooth width (mm) | 10 | | | | | | | |
| Peak-Peak Cogging torque (Nm) | 1.6 | 0.17 | 0.07 | 0.43 | 0.79 | 0.09 | 0.06 | 0.09 |
| Peak-Peak Cogging torque/ Average torque | 1.1 | 0.07 | 0.02 | 0.14 | 0.2 | 0.02 | 0.01 | 0.02 |
| Conventional E-core SFPM 6/11 | Average torque (Nm) 3.30 | | | | Torque density (kNm/m$^3$) 20.7 | | | |

Further, the saturation curve of the analysed machines is shown in Fig. 11(a) in terms of the torque variation with current density. The 11-rotor pole machine exhibits the largest torque profile under rated load condition compared to the other machines, although the 10-pole machines could withstand heavy overload than the rest of other machines, as seen from Fig. 11. Similarly, a comparison of the torque characteristics between the developed machine and conventional Ecore-SFPM machine presented in Fig. 11(b), shows that the developed machine is a more promising candidate with an amiable torque difference of about 11.4%. Furthermore, the predicted

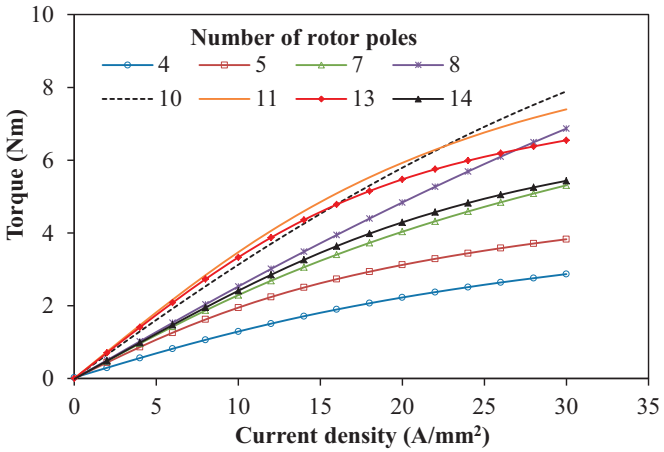


(a)

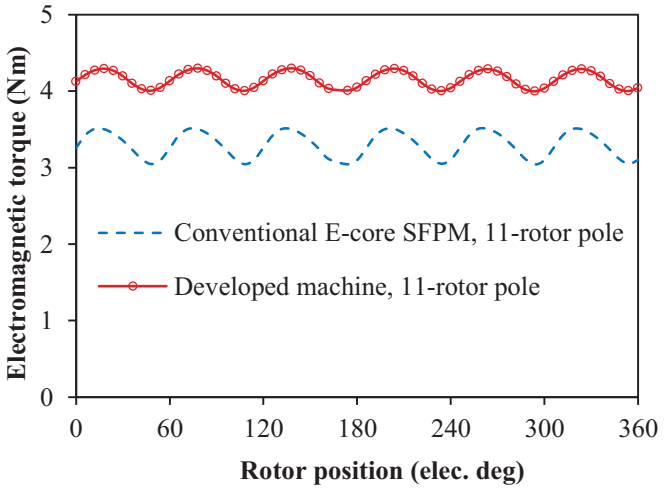


(b)

Fig. 11. Comparison of torque: (a) average torque versus current density; (b) electromagnetic torque versus rotor position

unbalanced magnetic force (UMF) in this paper is calculated using the Maxwell stress tensor approach with the expressions given in (10), (11) and (12) as stated in [27] and [28].

$$F_{\text{mag}} = \frac{1}{2\mu_o} \int_0^l \int_0^{2\pi} \left( B_{rd}^2 - B_{rq}^2 \right) r \, \mathrm{d}y \, \mathrm{d}x, \tag{10}$$

where: $B_{rd}$ and $B_{rq}$ are the $d$-and $q$-axes flux densities, respectively, $l$ and $r$ represent the radius from the air-gap, the axial stack length [27].

Similarly, the predicted $x$- and $y$ components of the forces acting on the rotor is given in (11) and (12).

$$F_x = \frac{rl}{2\mu_o} \int_0^{2\pi} \left[ \left( B_\alpha^2 - B_r^2 \right) \cos\alpha + 2B_r B_\alpha \sin\alpha \right] \mathrm{d}\alpha, \tag{11}$$

$$F_y = \frac{rl}{2\mu_o} \int_0^{2\pi} \left[ \left( B_\alpha^2 - B_r^2 \right) \sin\alpha - 2B_r B_\alpha \cos\alpha \right] \mathrm{d}\alpha, \tag{12}$$

where $B_\alpha$ and $B_r$ are the circumferential and radial components of the air-gap flux density [28].

It is stated in [29] that the UMF trajectory of a given electric machine would depend on the magnetic field harmonics owing to the nature and level of asymmetry or eccentricity of the rotor. Further, the machine geometry which includes the size of the back-iron, slot-opening, stator tooth-tip etc. has significant effect on the shape of the trajectory as proven in [30].

Furthermore, [28] stated that the resultant UMF waveform is also a function of both the directions and angular difference of the radial and tangential components of the forces acting on the rotor. From experience, the radial and tangential force components could be obtained separately from the FLUX / CEDRAT FEA software, unfortunately the two parameters are lumped together in the ANSYS-MAXWELL software employed in this analysis. It is worth mentioning that the obtained results in Fig. 13 are in accordance with the results presented in [28] and [31] of the conventional flux-switching PM machine, which shows that the trajectory must not be circular or spherical.

Also, Figs. 12–14 compare the variation of UMFs of the analysed machines under different load current and rotor positions, respectively.

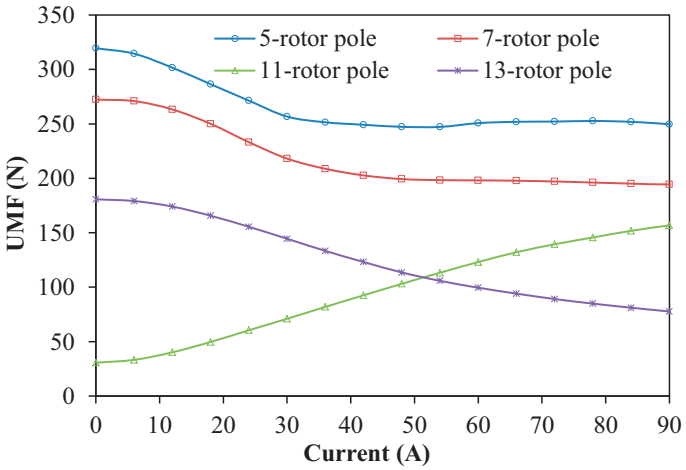


Fig. 12. Comparison of UMF in analysed machines, $i_d = 0$

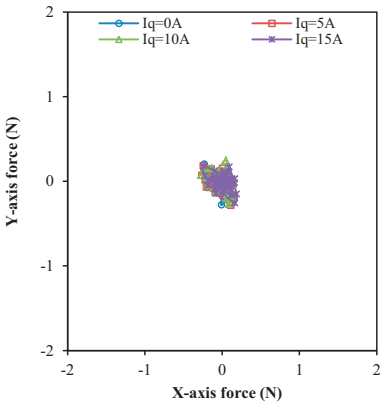


(a) 4-rotor pole

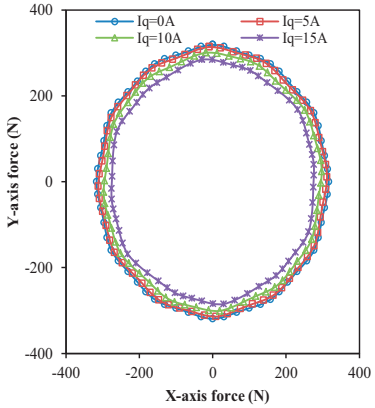


(b) 5-rotor pole

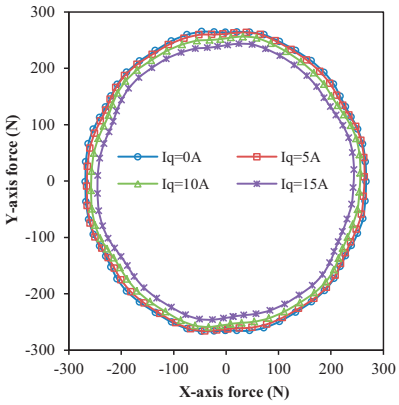


(c) 7-rotor pole

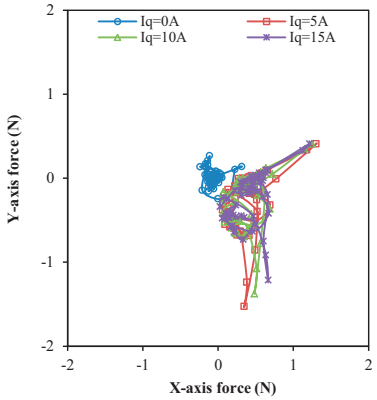


(d) 8-rotor pole

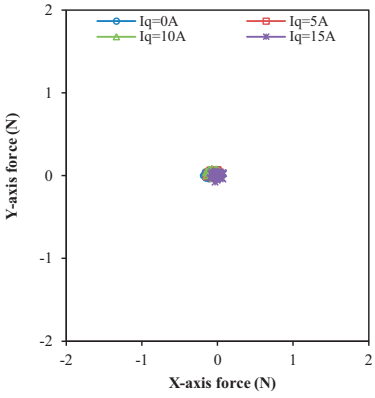


(e) 10-rotor pole

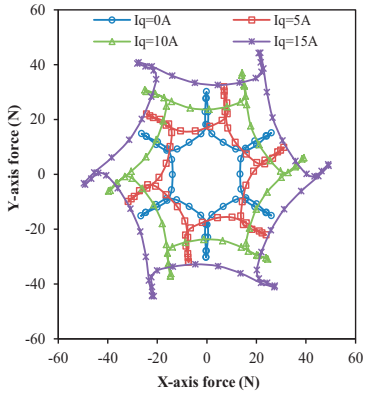


(f) 11-rotor pole

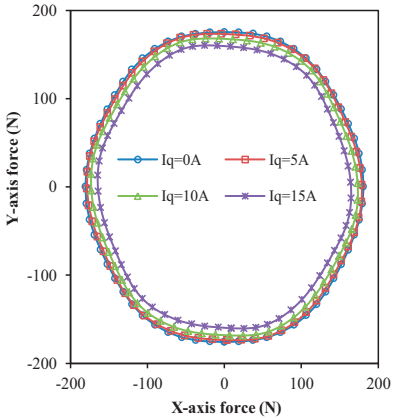


(g) 13-rotor pole

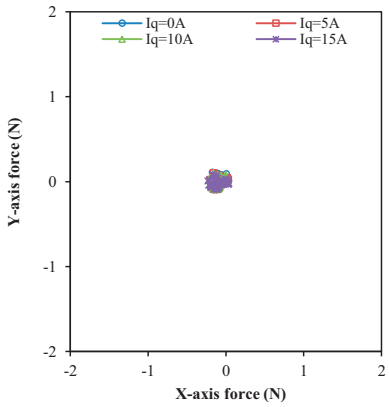


(h) 14-rotor pole

Fig. 13. Comparison of unbalanced magnetic force in analysed machines, $i_d = 0$

It is worth noting that, the largest amount of UMF occurs in the 5-pole machine; this is followed by the 7-pole machine. Whereas, the least amount of the UMF is obtained in the 11-pole machine. This unbalanced magnetic force effect on the rotor could be avoided by adopting an even number of rotor pole configurations; although it may lead to reduced machine performance. In general, a negligible amount of UMF is obtainable in machines having an even number of rotor poles due to its natural symmetrical characteristics compared to the odd rotor poles ones.

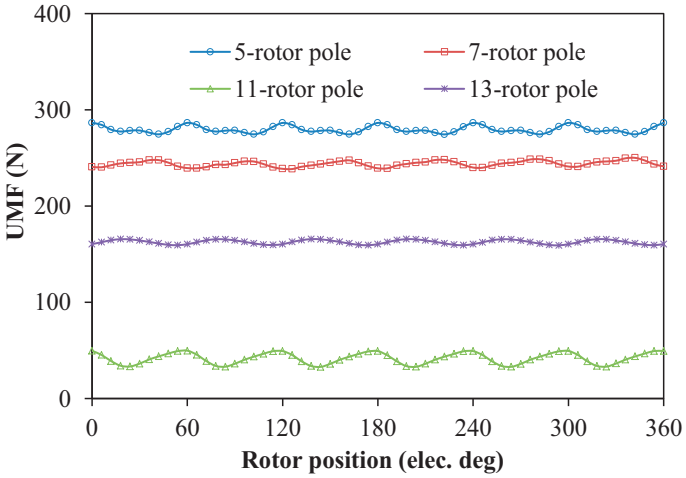


(a) Odd number of rotor poles

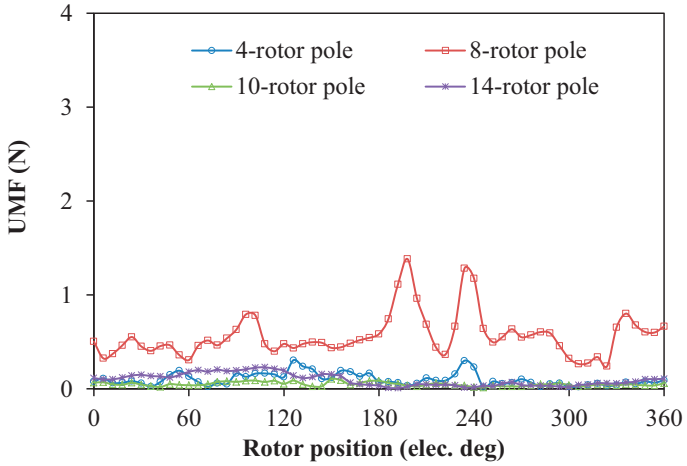


(b) Even number of rotor poles

Fig. 14. Variation of unbalanced magnetic force with rotor position, $I$ = 15 A

## 4. Conclusions

The analysis of cogging torque, torque ripple and total harmonic distortion of a flux-switching PM machine having two separate stators is investigated. Further, an account of unbalanced magnetic force on the rotor of the developed machine is also presented. The results reveal that, the four-rotor pole machine has the largest amount of undesirable features such as cogging torque, torque ripple and total harmonic distortion. More so, the frozen permeability result shows that the permanent magnet source contributes to a larger amount of flux-linkage, relative to that of the excited windings. Also, it is shown that the highest magnitude of unbalanced magnetic force on the rotor is obtained in the five-rotor pole machine. The analysed machine having an eleven-rotor pole number seems to have the most admirable qualities such as low UMF and a good torque density profile.

**Acknowledgements**

The first author would like to thank the Commonwealth Scholarship Commission, UK, for the sponsorship.

**References**

[1] Bianchini C., Immovilli F., Lorenzani E., Bellini A., Davoli M., *Review of design solutions for internal permanent magnet machines cogging torque reduction*, IEEE Transactions on Magnetics, vol. 48, no. 10, pp. 2685–2693 (2012).

[2] Lateb R., Takorabet N., Tabar F.M., *Effect of magnet segmentation on the cogging torque in surface-mounted permanent-magnet motors*, IEEE Transactions on Magnetics, vol. 42, no. 3, pp. 442–445 (2006).

[3] Fei W., Luk P.C.K., Shen J., *Torque analysis of permanent magnet flux switching machines with rotor step skewing*, IEEE Transactions Magnetics, vol. 48, no. 10, pp. 2664–2673 (2012).

[4] Liu T., Huang S., Gao J., Lu K., *Cogging torque reduction by slot-opening shift for permanent magnet machines*, IEEE Transactions on Magnetics, vol. 49, no. 7, pp. 4028–4031 (2013).

[5] Parsa L., Kim T., *Reducing torque pulsation of multi-phase interior permanent magnet machines*, Proceedings of 41st IEEE Industry Applications Annual Conference, Tampa, FL, USA, pp. 1978–1983 (2006).

[6] Ahn H., Jang G., Chang J., Chung S., Kang D., *Reduction of the torque ripple and magnetic force of a rotatory two-phase transverse flux machine using herringbone teeth*, IEEE Transactions on Magnetics, vol. 44, no. 11, pp. 4066–4069 (2008).

[7] Gong Y., Chau K.T., Jiang J.Z., Yu C., Li W., *Design of doubly salient permanent magnet motors with minimum torque ripple*, IEEE Transactions Magnetics, vol. 45, no. 10, pp. 4704–4707 (2009).

[8] Faiz J., Pakdelian S., *Finite-element analysis of a switched reluctance motor under static eccentricity fault*, IEEE Transactions on Magnetics, vol. 42, no. 8, pp. 2004–2009 (2006).

[9] Perers R., Lundin U., Leijon M., *Saturation effects on unbalanced magnetic pull in a hydroelectric generator with an eccentric rotor*, IEEE Transactions on Magnetics, vol. 43, no. 10, pp. 3884–3890 (2007).

[10] Zhang X., Liu X., Chen Z., *Investigation of unbalanced magnetic force in magnetic geared machine using analytical methods*, IEEE Transactions Magnetics, vol. 52, no. 7, ASN 8104504 (2016).

[11] Dorrell D.G., Popescu M., Ionel D.M., *Unbalanced magnetic pull due to asymmetry and low-level static rotor eccentricity in fractional-slot brushless permanent magnet motors with surface-magnet and consequent-pole rotors*, IEEE Transactions Magnetics, vol. 46, no. 7, pp. 2675–2685 (2010).

[12] Chen J.T., Zhu Z.Q., Howe D., *A dual-lumped parameter magnetic circuit model accounting for the cross-coupling effect, with particular reference to flux-switching permanent magnet machines*, Proceedings of 4th IET Conference on Power Electronics, Machines and Drives, York, UK, pp. 111–115 (2008).

[13] Chen J.T., Zhu Z.Q., Iwasaki S., Deodhar R.P., *A novel E-core switched flux PM brushless AC machine*, IEEE Transactions on Industry Applications, vol. 47, no. 3, pp. 1273–1282 (2011).

[14] Fasolo A., Alberti L., Bianchi N., *Performance comparison between switching-flux and IPM machines with rare-earth and ferrite PMs*, IEEE Transactions on Industry Applications, vol. 50, no. 6, pp. 3708–3716 (2014).

[15] Hua W., Zhang G., Cheng M., *Flux-regulation theories and principles of hybrid-excited flux-switching machines*, IEEE Transactions on Industrial Electronics, vol. 62, no. 9, pp. 5359–5369 (2015).

[16] Shuangxia N., Chau K.T., Dong Z., Jiang J.Z., Zheng W., *Design and control of a double-stator permanent-magnet motor drive for electric vehicles*, Proceedings of IEEE Industry Applications Annual Meeting, New Orleans, LA, USA, pp. 1293–1300 (2007).

[17] Shuangxia N., Chau K.T., Jiang J.Z., *A permanent-magnet double-stator integrated starter-generator for hybrid electric vehicles*, Proceedings of IEEE Vehicle Power and Propulsion Conference (VPPC), Harbin, China, pp. 1–6 (2008).

[18] Linni J., Guoqing X., Chunting C.M., Chau K.T., Chan C.C., *Analytical method for magnetic field calculation in a low-speed permanent-magnet harmonic machine*, IEEE Transactions on Energy Conversion, vol. 26, no. 3, pp. 862–870 (2011).

[19] Liu C., Chau K.T., Zhong J., Wenlong L., Fuhua L., *Quantitative comparison of double-stator permanent magnet vernier machines with and without HTS bulks*, IEEE Transactions on Applied Superconductivity, vol. 22, no. 3, ASN 5202405 (2012).

[20] Liu C., Chau K.T., Zhang Z., *Novel design of double-stator single-rotor magnetic-geared machines*, IEEE Transactions on Magnetics, vol. 48, no. 11, pp. 4180–4183 (2012).

[21] Awah CC., Zhu Z.Q., *Comparative study of high performance double-stator switched flux permanent magnet machines*, Proceedings of the 13th IEEE Vehicle Power and Propulsion Conference, Hangzhou, China, pp. 1–6 (2016).

[22] Chen J.T., Zhu Z.Q., Iwasaki S., Deodhar R.P., *Influence of slot opening on optimal stator and rotor pole combination and electromagnetic performance of switched-flux PM brushless AC machines*, IEEE Transactions on Industry Applications, vol. 47, no. 4, pp. 1681–1691 (2011).

[23] Chen J.T., Zhu Z.Q., *Winding configurations and optimal stator and rotor pole combination of flux switching PM brushless AC machines*, IEEE Transactions on Energy Conversion, vol. 25, no. 2, pp. 293–302 (2010).

[24] Evans D.J., Zhu Z.Q., *Novel partitioned stator switched flux permanent magnet machines*, IEEE Transactions on Magnetics, vol. 51, no. 1, ASN 8100114 (2015).

[25] Zhu Z.Q., Thomas A.S., Chen J.T., Jewell G.W., *Cogging torque in flux-switching permanent magnet machines*, IEEE Transactions on Magnetics, vol. 45, no. 10, pp. 4708–4711 (2009).

[26] Chandan S., Iqbal H., Wen O., *Cogging torque reduction in flux-switching permanent-magnet machines by rotor shaping*, IEEE Transactions on Industry Applications, vol. 51, no. 5, pp. 3609–3619 (2015).

[27] Jang S.M., Lee S.H., Cho H.W., Cho S.K., *Analysis of unbalanced force for high-speed slotless permanent magnet machine with halbach array*, IEEE Transactions on Magnetics, vol. 39, no. 5, pp. 3265–3267 (2003).

[28] Chen J.T., Zhu Z.Q., *Comparison of all and alternate poles wound flux-switching PM machines having different stator and rotor pole numbers*, IEEE Transactions on Industry Applications, vol. 46, no. 4, pp. 1406–1415 (2010).

[29] Burakov A., Arkkio A., *Comparison of the unbalanced magnetic pull mitigation by the parallel paths in the stator and rotor windings*, IEEE Transactions on Magnetics, vol. 43, no. 12, pp. 4083–4088 (2007).

[30] Pang Y., Zhu Z.Q., *Reduction of unbalanced magnetic force in 2-pole 3-slot permanent magnet machine*, Proceedings of 7th IET International Conference on Power Electronics, Machines and Drives, Manchester, UK, pp. 1–6 (2014).

[31] Lindner A., Hahn I., *Design of an E-core flux-switching permanent magnet machine with large air-gap*, Proceedings of IEEE International Electric Machines and Drives Conference, Coeur d'Alene, ID, USA, pp. 1580–1585 (2015).